Title
Relationship of DUX4 and target gene expression in FSHD myocytes

Journal
Human Mutation, 42(4)

ISSN
1059-7794

Authors
Chau, Jonathan
Kong, Xiangduo
Nguyen, Nam Viet
et al.

Publication Date
2021-04-01

DOI
10.1002/humu.24171

Peer reviewed

HHS Public Access

Author manuscript

Hum Mutat. Author manuscript; available in PMC 2022 April 01.

Published in final edited form as:

Hum Mutat. 2021 April ; 42(4): 421–433. doi:10.1002/humu.24171.

Relationship of *DUX4* and target gene expression in FSHD myocytes

Jonathan Chau[1,§], **Xiangduo Kong**[1,§], **Nam Nguyen**[1], **Katherine Williams**[2], **Rabi Tawil**[3], **Tohru Kiyono**[4], **Ali Mortazavi**[2,*], **Kyoko Yokomori**[1,*]

[1]Dept. Biol. Chem., School of Med., Univ. California, Irvine, CA

[2]Dept. Dev. Cell Biol., School of Biol. Sci., Univ. California, Irvine, CA

[3]Neuromuscular Disease Unit, Department of Neurology, University of Rochester Medical Center, Rochester, New York, USA

[4]Exploratory Oncology Research & Clinical Trial Center, National Cancer Center, Kashiwa City, Chiba, Japan

Abstract

Facioscapulohumeral dystrophy (FSHD) is associated with upregulation of the *DUX4* transcription factor and its target genes. However, low frequency *DUX4* upregulation in patient myocytes is difficult to detect and examining the relationship and dynamics of *DUX4* and target gene expression has been challenging. Using RNAScope *in situ* hybridization with highly specific probes, we detect the endogenous *DUX4* and target gene transcripts *in situ* in patient skeletal myotubes during 13-day differentiation *in vitro*. We found that the endogenous *DUX4* transcripts primarily localize as foci in one or two nuclei compared to accumulation of the recombinant *DUX4* transcripts in the cytoplasm. We also found the continuous increase of *DUX4* and target gene-positive myotubes after day 3 arguing against its expected immediate cytotoxicity. Interestingly, *DUX4* and target gene expression becomes discordant later in differentiation with the increase of *DUX4*-positive/target gene-negative as well as *DUX4*-negative/target gene-positive myotubes. Depletion of DUX4-activated transcription factors, DUXA and LEUTX, specifically repressed a DUX4-target gene, *KDM4E*, later in differentiation, suggesting that following the initial activation by DUX4, target genes themselves contribute to the maintenance of downstream gene expression. Together, the study provides important new insights into dynamics of DUX4 transcriptional network in FSHD patient myocytes.

Keywords

FSHD; DUX4; LEUTX; KDM4E; RNAScope; skeletal myotubes

[*]co-corresponding authors: Ali Mortazavi, 2218 Biological Sciences III, Department of Developmental and Cell Biology, School of Biological Sciences, University of California, Irvine, CA92697-2300, U.S.A.; TEL: 949-824-6762; ali.mortazavi@uci.edu; Kyoko Yokomori, 240D, Medical Sciences I, Department of Biological Chemistry, School of Medicine, University of California, Irvine, CA92617-1700, U.S.A.; TEL: 949-824-8215; kyokomor@uci.edu.

[§]co-first authors.

Conflict of Interest: NIL

Introduction

Facioscapulohumeral dystrophy (FSHD) is an autosomal dominant muscular dystrophy initiating with progressive wasting of facial, shoulder, and upper arm musculature (van der Maarel & Frants, 2005). It is one of the most common muscular dystrophies (1 in 8,333) (Deenen et al., 2014). The majority of FSHD cases (>95%) are linked to monoallelic deletion of D4Z4 macrosatellite repeat sequences at the subtelomeric region of chromosome 4q (4qter D4Z4) (termed FSHD1 (MIM# 158900)) (van der Maarel & Frants, 2005; van der Maarel, Tawil, & Tapscott, 2011). Only one to ten D4Z4 repeats are found in the contracted allele in FSHD1 while 11~150 copies are present in the intact allele. FSHD2 is the rare form of FSHD (<5% of cases) with no D4Z4 repeat contraction but exhibits the clinical phenotype identical to FSHD1 (de Greef et al., 2010). Recent studies have found that the *SMCHD1* gene is mutated in >80% of FSHD2 cases (MIM# 158901) (Lemmers et al., 2012) as well as in severe cases of FSHD1 (Larsen et al., 2015; Sacconi et al., 2013). Mutations of DNMT3b and LRIF1 have also been linked to FSHD2 (Hamanaka et al., 2020; van den Boogaard et al., 2016).

D4Z4 is a 3.3 kb repeat containing an open reading frame for the double-homeobox transcription factor (TF) *DUX4* gene (Gabriëls et al., 1999; Geng et al., 2012; Snider et al., 2010). *DUX4* is essential during early embryogenesis but is subsequently silenced (De Iaco et al., 2017; Hendrickson et al., 2017; Whiddon, Langford, Wong, Zhong, & Tapscott, 2017). Only individuals with a 4qA haplotype with a non-canonical polyadenylation signal sequence for the *DUX4* transcript distal to the last D4Z4 repeat express a full-length *DUX4* transcript (*DUX4fl*) and develop FSHD (Lemmers et al., 2010). Expression of *DUX4fl* is closely associated with FSHD, which strongly suggests that *DUX4* expression is critical for FSHD pathogenesis (Himeda, Jones, & Jones, 2015; Lemmers et al., 2010; Snider et al., 2010). Activation of many, if not all, DUX4 target genes has been observed in patient cells in multiple studies, supporting the significance of *DUX4fl* in FSHD. However, how dysregulation of any of these target genes directly contributes to the disease process is still under active investigation (Broucqsault et al., 2013; Ferreboeuf, Mariot, Bessières, et al., 2014; Geng et al., 2012; Jones et al., 2012; Rahimov et al., 2012; Rickard, Petek, & Miller, 2015).

Curiously, the *DUX4fl* transcript is expressed at extremely low levels and sometimes is not detectable (Jones et al., 2012; Snider et al., 2010), and DUX4 protein is detectable only in <0.1% of patient muscle cells (Himeda et al., 2015; Lemmers et al., 2010; Snider et al., 2010; Tsumagari et al., 2011). Furthermore, *DUX4fl* expression can occasionally be observed even in unaffected individuals (Jones et al., 2012; Snider et al., 2010). Although overexpression of the recombinant DUX4 in *in vitro* myoblasts and *in vivo* in model organisms was shown to be toxic (Bosnakovski et al., 2008; Vanderplanck et al., 2011), recent evidence indicates that the phenotype induced by the recombinant overexpression can differ from that of the endogenous DUX4 (Homma, Beermann, Boyce, & Miller, 2015). Thus, there is a critical need to study the effect of the endogenous *DUX4* expression. However, assessment of the endogenous *DUX4* and target gene expression in FSHD patient myocytes has been limited. Recently, we detected *DUX4* and target gene transcripts using single-nucleus RNA sequencing (snRNA-seq) (Jiang et al., 2020). Unlike the previous single

cell RNA-seq of fusion-blocked myotubes (van den Heuvel et al., 2019), our isolation and analyses of nuclei from naturally fused multi-nucleated myotubes provided the first evidence that DUX4 target gene expression is much more wide-spread than *DUX4* transcription itself, which explains easier detection of the target gene transcripts rather than *DUX4* itself (Broucqsault et al., 2013; Ferreboeuf, Mariot, Bessières, et al., 2014; Geng et al., 2012; Jones et al., 2012; Rahimov et al., 2012; Rickard et al., 2015). SnRNA-seq was highly instrumental in defining the different states of FSHD patient myocyte nuclei distinct from those of control myocyte nuclei. However, it failed to provide spatial relationship of individual nuclei and associated gene expression. In the current study, we examined the spatiotemporal relationship between the expression of *DUX4* and some of its major target genes in control and FSHD myocytes during differentiation using RNAScope, an *in situ* hybridization assay for RNA detection (Wang et al., 2012). We designed the probe set that maximizes the potential to detect *DUX4fl* and minimizes the crossreactivity with other isoforms and related genes. Our results reveal unique nuclear accumulation of the endogenous *DUX4* transcript distinct from the recombinant *DUX4* RNA, and increase of the endogenous *DUX4* and target gene transcripts over time arguing against immediate cytotoxicity. Interestingly, DUX4 and target gene expression becomes discordant and LEUTX, a primate-specific DUX4 target TF, contributes to the efficient activation of another DUX4 target *KDM4E*. These results reveal dynamic DUX4 and target gene network, and serve as an important basis for further understanding of the FSHD pathogenesis.

Methods

Cell culture and differentiation

Primary and immortalized control, FSHD1 and FSHD2 skeletal myoblast cells were grown in high glucose DMEM (Gibco) supplemented with 20% FBS (Omega Scientific, Inc.), 1% Pen-Strep (Gibco), and 2% Ultrasor G (Crescent Chemical Co.). Primary control and FSHD2 (4qA161, *SMCHD1* mutation: g.2697999_2698003del) myoblasts (Jiang et al., 2020) as well as FSHD1 (4qA161, 2 D4Z4 units) myoblasts were immortalized using hTERT with p16INK4a-resistant R24C mutant CDK4 (mtCDK4) and Cyclin D1 as previously described (Shiomi et al., 2011). After immortalization, CD56-positive cells were selected by magnetic-activated cell sorting conjugated with anti-CD56 antibody (130–050-401, MiltenyiBiotec). Single cell clones were isolated by FACS sorting into 96 well plates. Control, FSHD1 and FSHD2 clones were chosen for the experiments based on normal doubling time and high differentiation index. Myoblast differentiation was induced as previously described (Zeng et al., 2016). Briefly, cells were plated at a seeding density of ~2.5×10^5 cells/ml in 0.5 ml of growth medium in each well of a 24-well dish. Approximately 12–16 hr later differentiation was induced using high glucose DMEM medium supplemented with 2% FBS and ITS supplement (insulin 0.1%, 0.000067% sodium selenite, 0.055% transferrin, 51300044 Invitrogen). Fresh differentiation medium was changed every day.

Antibodies and cDNA clone

Immunofluorescence was performed using rabbit polyclonal antibodies specific for DUX4 (ab124699, Abcam) and LEUTX (PA5–59595, Thermofisher). DUX4 shRNA treatment

reduced this DUX4 antibody staining by ~80%, supporting the specificity (data not shown). The recombinant DUX4 expression plasmid (pCS2-mkgDUX4) was a gift from Dr. Stephen Tapscott (Addgene plasmid # 21156) (Snider et al., 2009).

RNAScope probe design

The following RNAScope probes (Advanced Cell Diagnostics, Inc.) were used: *LEUTX* (Hs-LEUTX-C2, Cat No. 547251-C2), *KDM4E* (Hs-KDM4E-C3, Cat No. 556121-C3), *SLC34A2* (Hs-SLC34A2-C3, Cat No. 407101-C3), *ZSCAN4* (Hs-ZSCAN4-C2, Cat No. 421091-C2) and 15ZZ *DUX4* (Hs-DUX4-No-XMm-C3, Cat No. 498541-C3). The 6ZZ *DUX4fl* probe set (HS-DUX4-O6-C1, Cat No. 546151) was specifically designed for *DUX4fl* (NM_001306068.2), with only 1 or 2 ZZ pairs residing in the regions shared with *DUX4s* or *DUX4c* (at least 3ZZs are needed for signal detection) (Fig. 1A).

RNAScope hybridization

Cells were grown and differentiated on cover slips in 24-well plates. Cells were washed twice with PBS, then fixed with 10% neutral buffered formalin (NBF) for 30 min at room temperature (RT), and finally dehydrated with 50%, 70%, and 100% ethyl alcohol gradients for 1 min each at room temperature. Cells were then rehydrated with 70% and 50% ethyl alcohol gradients for 1 min each and finally treated with PBS for 10 min. Cells were then treated with hydrogen peroxide (Cat No. 322335 ACDBio) and protease III (Cat No. 322337 ACDBio) at RT for 10 min each and washed with PBS. The probe sets for *DUX4*, *LEUTX*, *KDM4E* were then added in a 50:1:1 ratio for 2 h at 40°C within a humidity control chamber. Probe sets are optimized for different fluorescent channels (C1, C2, and C3, respectively). RNAScope multiplex signal amplification (Cat No. 323110 ACDBio) were applied sequentially and incubated in AMP 1, AMP 2, AMP 3 for 30, 30, 15 min respectively at 40°C within the humidity control chamber. Before adding each AMP reagent, cells were washed twice with RNAScope washing buffer (Cat No. 310091 ACDBio). Signal was developed with the Fluorescent Detection Reagents (Cat No. 323110 ACDBio) and TSA Plus Fluorophores diluted 1:1500 in RNAScope TSA Buffer (Cat No. 322810 ACDBio). To develop C1 signal, samples were incubated in HRP-C1, TSA Plus Fluorescein (cat. No. NEL741001KT PerkinElmer), HRP Blocker for 15, 30, 15 min, respectively, at 40°C within the humidity control chamber. Before adding each reagent, cells were washed twice with RNAScope washing buffer. For C2 and C3 costaining, TSA Plus Cy 3 and Cy 5 were used, respectively (cat no. NEL744001KT and NEL745001KT PerkinElmer). Cells were then counterstained with DAPI (Cat No. 320858 ACDBio) for 30s at RT and washed twice with PBS. Samples were then dried and mounted onto microscope slides with ProLong Diamond Antifade Mountant (Cat No. P36961 ThermoFisher).

Immunofluorescent co-staining with RNAScope (immuno-RNAScope)

Cells were grown and differentiated on coverslips in 24-well plates. For costaining of DUX4 antibody and *DUX4* RNAScope probes, cells were fixed with 10% NBF for 30 min at RT and then extracted with 0.5% Triton X-100 in PBS. Primary and secondary antibodies were diluted in SNBP (1XPBS /0.02% saponin /0.05% NaN_3 /1% BSA), containing 1% horse serum and 0.05% gelatin. Samples were incubated in primary antibody for 30 min at 37°C followed by three PBST (PBS with 0.05% Tween20) washes. Coverslips were incubated in

secondary antibody for 30 min at 37°C followed by three PBST washes. Cells were then dehydrated with 50%, 70%, and 100% ethyl alcohol gradients for 1 min each at RT and continued to be processed for RNAScope hybridization as described above. Then coverslips were counterstained with DAPI, washed with dH_2O and mounted with Prolong Diamond Antifade Mountant. For costaining of LEUTX protein and *LEUTX* RNA, the RNAscope protocol was done before the immunofluorescence. Before DAPI counterstaining in the RNAscope procedure, coverslips were blocked in PBST, containing 2% BSA and 10% Milk for 45 min. Primary and Secondary antibodies were diluted in the blocking buffer. Samples were incubated in primary antibody for 2h at RT followed by three PBST washes. Coverslips were then incubated in secondary antibody for 1h at RT followed by three PBST washes. Then, coverslips were counterstained with DAPI, washed with PBST and mounted with Prolong Diamond Antifade Mountant. The costaining of LEUTX protein and *KDM4E* RNA was done according to the protocol "RNAscope Multiplex Fluorescent V2 Assay combined with immunofluorescence" provided by ACDBio.

Fluorescent image acquisition, quantification and statistical analysis

Images were acquired with a Zeiss LSM510 confocal laser microscope. On the 12 mm diameter coverslip, 5 horizontal sections were observed and myotubes were counted. Three replicates were done of each staining experiment and error bars were calculated using standard deviation from the mean. ImageJ software was used to quantify *KDM4E* RNAScope and LEUTX antibody staining signals in LEUTX and DUXA depletion experiments. Briefly, line was drawn around each myotube, and the fluorescent signal was measured inside of the line as the mean gray value and the average background mean gray value from three different negative myotubes was subtracted. Because so few myotubes were positive for *KDM4E* RNA and LEUTX protein to begin with, and to be more comparable with RT-qPCR results, the integrated density (the total *KDM4E* RNA or LEUTX protein signal in each myotube) was then back-calculated as the mean intensity multiplied by the area of each myotube. The integrated density values of top 5% myotubes (corresponding to 25 myotubes out of 500 myotubes examined) amount to >95 % of the total *KDM4E* RNA or LEUTX protein signals in control shRNA-treated myotubes. Thus, top 5% values in each group were used for graph and data analysis. Arbitrary numbers in Y-axis was obtained by normalizing all the data to the mean value of the control shRNA samples.

ShRNA depletion and RT-qPCR

Lentiviruses carrying shRNA plasmids (MISSION shRNA, Sigma-Aldrich) for each DUX4 target gene: *DUXA* (5'-CTAGATTACTTCTCCAGAGAA-3', TRCN0000017664), *LEUTX* (5'-CCTGGAATCTCTGATGCAAAT-3', TRCN0000336862), and an shRNA control (SHC002) were made in 293T cells using Lipofectamine P3000. The cells were transfected with 2 μg of shRNA plasmids, 1.5 μg of pCMV plasmids, and 0.5 μg of pMP2G plasmids (Sikandar et al., 2010). The media was changed after 24 hours. The lentiviruses were harvested at 48 hour and 72 hour post-transfection. FSHD2 immortalized myoblasts were infected twice at 32 hour and 8 hour prior to differentiation. The myoblasts were selected with puromycin. The RNA was extracted using RNeasy kit (Qiagen, Cat No. 74134) at days 4 and 6. Around 16 ng of RNA was converted to cDNA using SuperScript IV VILO Master (Thermofisher, Cat No. 11756050) and then used for RT-qPCR analysis. PCR primers are

listed in Supplemental Table S1. Cells were also subjected to immuno-RNAScope as described above.

Detection of apoptosis in control and FSHD cells

Apoptosis in immortalized control and FSHD myocytes at day 3 of differentiation was detected using the commercial kit (AB176749; Abcam, Cambridge, England) following the manufacturer's instructions. In apoptotic cells, phosphatidylserine (PS) is transferred to the outer side of the plasma membrane and can be detected by its sensor, Apopxin Green (green fluorescence). Live cells can be detected as blue fluorescence by CytoCalcein Violet 450 staining. The percentage of Apopxin Green area in total area was quantified using the Analyze Particles module of ImageJ software.

Statistical Analyses

Microsoft Excel software was used to perform statistical analyses on data from three independent experiments. The statistical significance is determined by the Student's t-test. $P < 0.05$ is considered of statistical significance. The error bars denote standard deviation. Phi (φ) coefficient (analytically equivalent to Pearson's correlation for binary data) is calculated following the previous paper (Mainali et al., 2017). φ takes on values ranging between +1 and −1. The following points are the accepted guidelines for interpreting the correlation coefficient: "$\varphi=1$", "$1>\varphi>0.5$", "$0.5>\varphi>0.3$" and "$0.3>\varphi>0.1$" indicate perfect, strong, moderate and weak positive relationship respectively; "$0.1>\varphi>-0.1$" indicates no relationship; while "$\varphi=-1$", "$-1<\varphi<-0.5$", "$-0.5<\varphi<-0.3$" and "$-0.3<\varphi<-0.1$" indicate perfect, strong, moderate and weak negative relationship respectively.

Results and Discussion

DUX4 RNA accumulates in the nucleus of the FSHD myotubes

Multiple *DUX4* homologs and isoforms are known to be expressed in human myocytes (Snider et al., 2010). In particular, *DUX4s and DUX4c* were shown to be expressed more widely than *DUX4fl* even in control cells (Ansseau et al., 2009; Snider et al., 2010) (Supplemental Figure S1). Thus, to minimize crossreactivity and maximize the preferential detection of the full length *DUX4 (DUX4fl)* shown to be most relevant to FSHD, we custom designed an RNAScope probe set with the lowest possible number of ZZ probe pairs ("ZZ" represents a pair of RNAScope target probes) for the fluorescent detection system (Fig. 1A; 6ZZ). Interestingly, we observed the major *DUX4* transcript signal as foci in the nucleus using this set in primary FSHD myotubes (Fig. 1B) (Jiang et al., 2020).

Unlike our probe set, previous studies using either a conventional FISH probe or another RNAScope probe set (ACDBio cat. no. 498541) detected *DUX4* transcript signals in the cytoplasm (Amini Chermahini, Rashnonejad, & Harper, 2019; Ferreboeuf, Mariot, Furling, et al., 2014). To address this apparent discrepancy, we performed costaining of the two RNAScope probe sets. The previous probe set was designed for the colorimetric DAB staining (Amini Chermahini et al., 2019), which does not allow costaining. Thus, we remade the previous probe set compatible with fluorescent labeling and performed costaining with our new 6ZZ probe set. As expected, fluorescent labeling does not give as strong a signal as

DAB (Fig. 1B) (Amini Chermahini et al., 2019). Since the previous *DUX4* probe set contains 15 ZZ pairs (thus designated 15ZZ), the fluorescent signal is stronger than our 6ZZ probe set (Fig. 1B and C). Weaker staining by 6ZZ is due to fewer ZZ pairs in our probe set in order to minimize the potential crossreactivity to *DUX4s and DUX4c* (Fig. 1A). In the 15ZZ probe set, 3 and 5 ZZ pairs reside in two sub-regions of *DUX4fl* RNA shared by *DUX4s* and *DUX4c* transcripts, enabling 4ZZ and 6ZZ pairs to cross-hybridize *DUX4s* and *DUX4c*, respectively (Fig. 1A; 15ZZ). Consistent with this, 15ZZ shows some staining in control cells, in contrast to no significant signal by 6ZZ (Fig. 1C). It is therefore possible that some of the signals detected by the 15ZZ probe set may come from that of *DUX4s* and/or *DUX4c*. Nevertheless, we found close colocalization of major fluorescent signals at nuclear foci by both probe sets, confirming the significant retention of *DUX4* transcripts in the nucleus (Fig. 1B). Some nuclear staining was also apparent in Figure 2C in the previous paper (Amini Chermahini et al., 2019) though it was less clear due to the dark nuclear hematoxylin staining. We further confirmed the presence of DUX4 protein in the same myotube that contains the endogenous *DUX4* transcript-positive nuclei (Fig. 1D). Consistent with previous observations (Jiang et al., 2020; Rickard et al., 2015; Tassin et al., 2013), expression of *DUX4* RNA transcripts in even one nucleus appears to be sufficient for DUX4 protein localization in most of the nuclei in the same myotube. Taken together, these results strongly support the specificity of the 6 ZZ probe set and indicate that the majority of *DUX4* transcripts are retained in the nucleus forming foci in FSHD myotubes.

Cytoplasmic signals can also be observed by the 15ZZ probe set and weakly by ours in some FSHD myotubes with higher expression of endogenous *DUX4* (Fig. 1B, indicated by arrowheads). Since the cytoplasmic localization of the recombinant *DUX4* (*recDUX4*) transcript was observed previously (Amini Chermahini et al., 2019), we also examined the localization of *recDUX4* transcript. Indeed, we found that the overexpressed rec*DUX4* transcript is highly localized in the cytoplasm with much less nuclear localization (Fig. 1E). It is currently unclear whether this different RNA localization pattern is simply due to vast overexpression of the recombinant *DUX4* or possibly due to differences in template sequences and/or gene locations (ectopic vs. genomic). It is possible, for example, that untranslated regions, which are missing in the recombinant *DUX4* construct, may dictate the nuclear localization of the endogenous *DUX4* transcript. Nevertheless, the results revealed the significant difference between the endogenous and overexpressed recombinant *DUX4* transcript localization, highlighting the distinct retention in the nucleus of *DUX4* RNA transcribed from the endogenous locus.

Quantification of *DUX4fl*-expressing nuclei in immortalized FHSD myotubes

To perform systematic analyses of *DUX4* and target gene transcripts, we established immortalized control and FSHD2 myoblast lines using *hTERT*, mutant *CDK4* and *CCND1* as described previously (Zeng et al., 2016). We chose one particular FSHD2 patient myoblast sample for immortalization because of the significant expression of *DUX4* and target genes, which were previously demonstrated by bulk RNA-seq and snRNA-seq during the first 5 days of differentiation (Jiang et al., 2020). After immortalization and surface marker isolation, several single clones were characterized and compared, and one of them that retained high proliferation and differentiation capabilities was chosen and used for the

rest of the study. When this cell line was differentiated into myotubes for 4 days (Fig. 2A), we observed similar nuclear foci of *DUX4* RNA by both 15ZZ and 6ZZ probe sets as in primary cells (Fig. 1), indicating that immortalization did not affect *DUX4* RNA expression and localization (Fig. 2B). We further quantified *DUX4* RNA signals detected by 6ZZ in control and FSHD myotubes. No signal was detected in control myotubes (N=348) (Fig. 2C). We observed *DUX4* RNAScope signals in one to two nuclei in ~2.8% of FSHD2 myotubes on average (N=414) (Fig. 2C). Comparable *DUX4* RNAScope signal patterns and frequencies were observed in both primary parental and corresponding immortalized myotubes (Figs. 1 and 2) (Jiang et al., 2020). Similar to the primary cells, we observed that multiple nuclei in a myotube are positive for DUX4 protein when only a few nuclei express *DUX4* RNA (Figs. 1D and 2D).

Time course analyses of *DUX4* and target gene transcripts

To examine the relationship between DUX4 and its target transcripts, we designed probes for *LEUTX, KDM4E, ZSCAN4*, and *SLC34A2* transcripts known to be activated by DUX4 (Jagannathan et al., 2016; Rickard et al., 2015; Yao et al., 2014). We found specific expression of *LEUTX*, *KDM4E*, and *ZSCAN4* using our RNAScope probe sets in FSHD myotubes in a frequency similar to that of *DUX4* (Figs. 2C and 3A). Quantification of these stainings is shown on the right (Fig. 3A). We failed to detect any significant target gene signals in undifferentiated myoblasts (data not shown). Unlike *DUX4*, however, these target gene transcripts, if expressed, accumulate abundantly in the cytoplasm (Fig. 3A). The probe set for *SLC34A2* detected strong cytoplasmic signals in FSHD myotubes (Fig. 3A). However, some non-specific staining was seen in control cells, and thus the probe set appears to be not completely specific to FSHD-induced *SLC34A2* RNA (data not shown). Thus, we eliminated this probe from further analyses. We confirmed the presence of LEUTX protein in all the nuclei in the same myotube with *LEUTX* RNA signal, confirming the correlation of RNA and protein expression (Fig. 3B, middle). Quantification of these different patterns is shown on the right (Fig. 3B). We observed one myotube with weak LEUTX protein staining and no RNA (Fig. 3B, bottom). It is unclear whether this represents a myotube with residual LEUTX protein after mRNA transcription was ceased. With these results, we chose *LEUTX* and *KDM4E* transcripts for further time course analyses.

While the upregulation of DUX4 target genes in FSHD is relatively well established, how *DUX4* activation results in target gene expression during human myoblast differentiation has not been studied at the single cell level in the context of the natively fused myotubes. Previous work to understand this question includes single cell RNA-seq done on fusion-inhibited myocytes (van den Heuvel et al., 2019) and our recent single-nucleus RNA-seq (Jiang et al., 2020). However, neither study was able to address the relationship of *DUX4* and target gene expression in the intact myotube. Thus, we performed triple staining for endogenous *DUX4*, *LEUTX, and KDM4E* expression to investigate their localization *in situ* during differentiation from day 3 through day 13 (Fig. 4 and Supplemental Figure S2). Because the number of all *DUX4* and target gene-expressing myotubes is limited (typically ~2% for days 3–5 and ~5% for later days of the entire myotube population on a coverslip), obtaining statistically significant quantification data is challenging. Nevertheless, with multiple experimental replicates, we were able to observe a reproducible trend for *DUX4*

and target gene expression kinetics during differentiation (Fig. 4B). Previously, we followed the increase of DUX4 target gene induction up to 5 days of differentiation by RNA-seq (Jiang et al., 2020). In the current study, we observed that the number of myotubes expressing target genes (*LEUTX* and/or *KDM4E* with or without *DUX4)* has a tendency to increase throughout the duration of a 13-day time course (Fig. 4C, pink and blue). Increasing trajectory of *DUX4* and target gene-positive myotubes argue against the previous suggestion that *DUX4* expression leads to immediate cell death (Rickard et al., 2015; Shadle et al., 2017). We also found that the number of myotubes with *DUX4* only expression (without any target gene expression) increases significantly starting at day 3 and peaks at day 7 (Fig. 4B and C green), indicating that there are two states of *DUX4*-positive myotubes (with or without downstream gene activation). The results raise the possibility that an additional factor(s) may be involved in efficient downstream target gene activation.

Unexpectedly, the number of myotubes expressing two target genes (*LEUTX* and/or *KDM4E*) without *DUX4* increased later in differentiation (Fig. 4C blue), suggesting their continued upregulation with no *DUX4* transcripts present. Consistent with this, the frequency of *LEUTX* coexpression with *DUX4* decreases significantly later in differentiation (Fig. 4D). These results strongly suggest that for those myotubes in which the target genes are activated (initially by DUX4), their expression may continue even when *DUX4* expression is not maintained. We also followed the expression of *ZSCAN4* with *DUX4* and *KDM4E* and observed a significant decrease of *ZSCAN4* coexpression with *DUX4* (Fig. 4E; Supplemental Fig. S3), indicating that this is not a limited phenomenon for *LEUTX*. To further validate this, we immortalized FSHD1 myoblasts using the same strategy. Using these cells, similar results were obtained as in FSHD2 myocytes, indicating that this is not restricted to FSHD2 with SMCHD1 mutation (Fig. 4F–H; Supplemental Figure S4). This particular cell line undergoes myotube fusion ~1 day earlier than the FSHD2 line and thus, the peak of *DUX4* and target gene expression occurs earlier than the FSHD2 line used in this study (Fig. 4F). Nevertheless the appearance of myotubes expressing *DUX4* without *LEUTX/KDM4E* and those with *LEUTX/KDM4E* without *DUX4* (Fig. 4G), and discordance of *LEUTX* and *DUX4* expression are comparable (Fig. 4H). Taken together, the results reveal some discordance between *DUX4* and target gene RNA expression, suggesting the possible presence of additional regulatory mechanisms for sustained *DUX4* gene network activation in FSHD patient myocytes.

KDM4E expression is regulated by DUXA and LEUTX

The above results reveal coexpression of DUX4 target genes in the same myotubes with no detectable *DUX4* (Fig. 4B and C; Fig. 4F and G). In FSHD2 cells, the number of *KDM4E* expressing myotubes increases even after *DUX4* expression peaks at day 7 (Fig. 5A). Coexpression of *KDM4E* and *LEUTX* without *DUX4* increases later in differentiation (Fig. 4C, blue) and *KDM4E* transcript expression correlates better with expression of *LEUTX* than *DUX4* (Fig. 5B). Costaining of LEUTX protein with *KDM4E* transcripts on day 6 revealed that all observed *KDM4E* staining co-localized with LEUTX protein staining in the same myotubes (Supplemental Fig. S5). For FSHD1 cells that we used, the expression profiles are little different possibly due to differences in differentiation efficiency (see above) (Fig. 5C). Nevertheless, colocalization of *KDM4E* with *LEUTX* expression in the same

myotube is consistently better than with *DUX4* expression (Fig. 5D). Motif analyses revealed that the promoter region of the *KDM4E* gene contains not only the DUX4 binding motif, but also multiple sites of the putative LEUTX binding motif (Supplemental Fig. S6) (Jouhilahti et al., 2016; Katayama et al., 2018). These results raise the possibility that LEUTX may be involved in *KDM4E* upregulation. We recently found that DUXA, another DUX4 target, plays a significant role in upregulating *LEUTX* later in differentiation in FHSD2 myocytes (Jiang et al., 2020). Thus, we depleted LEUTX and DUXA by shRNAs in FSHD2 myocytes (Fig. 5E). Because of the difficulty detecting DUXA and LEUTX proteins by western blot, depletion efficiency was confirmed by RT-qPCR (Fig. 5F). Although depletion efficiency is at a comparable level on day 4 and day 6 of differentiation, LEUTX and DUXA depletion specifically repressed *KDM4E* expression on day 6, but not day 4. To further substantiate the results, we also assessed the depletion effects using antibody specific for LEUTX and RNAScope for *KDM4E* on day 6 (Fig. 5G). The results are consistent with RT-qPCR results, demonstrating significant reduction of *KDM4E* RNA together with LEUTX protein depletion in LEUTX shRNA-treated myotubes. Interestingly, LEUTX protein-positive *KDM4E* RNA-negative myotubes were observed in DUXA-depleted myotubes, supporting the idea that DUXA may stimulate KDM4E expression directly. Consistent with this, several DUXA motifs are found in the *KDM4E* gene region, and the DUX4 binding motif in the promoter may be similar enough to be bound by DUXA (Supplemental Fig. S6A and B). Taken together, these results indicate that LEUTX (and DUXA either directly or indirectly through LEUTX upregulation) promotes *KDM4E* expression following the initial activation by DUX4 (Fig. 5H). The results support our hypothesis that once activated, the DUX4 target genes may in part self-sustain their expression (Jiang et al., 2020).

Detection of the endogenous *DUX4* expression and its relationship with its target gene expression in patient myocytes has been technically challenging due to the low frequency of *DUX4*-expressing cells. Here we use a custom-designed RNAScope probe set to maximize the detection of the pathogenic full-length *DUX4* transcript and to analyze its localization and relationship with its downstream target genes in differentiating FSHD myotubes. The use of RNAScope ((Amini Chermahini et al., 2019) and the current study) provides a complementary tool to single-cell/nucleus RNA-sequencing to understand FSHD pathogenesis with high spatiotemporal resolution. Our results reveal snapshots of FSHD-induced gene expression in patient myocytes during 13-day differentiation, a duration much longer than previously examined, and provide new insight into gene expression changes in patient myocytes. We discovered that the endogenous *DUX4* RNA mainly accumulates in the nucleus, which is in stark contrast to the recombinant *DUX4* RNA that abundantly accumulates in the cytoplasm. We also found that *DUX4* expression increases over a week of differentiation, suggesting that it is not immediately toxic. Unlike the immediate cytotoxic effect of the recombinant DUX4 overexpression, we also failed to observe any significant signs of apoptosis compared to the control myocytes under our condition on day 3 of differentiation (Supplemental Fig. S7), which is consistent with apparent lack of apoptotic transcriptomic signature during the first 5 days (Jiang et al., 2020). It would be interesting to speculate that retention of *DUX4* transcripts in the nucleus may be one way for the cell to control the expression of DUX4 to avoid cytotoxicity. Importantly, our long time course

analyses uncovered that *DUX4* and target gene expression are not always concordant in individual myotubes, identifying different states of DUX4-activated patient myotubes. Once activated by DUX4, LEUTX and DUXA, to a certain extent, appear to contribute to sustaining DUX4-induced *KDM4E* activation. We previously showed DUXA also stimulates expression of *ZSCAN4* (Jiang et al., 2020). Taken together, our findings further substantiate an additional layer of regulation to the DUX4-induced transcriptional network and provide an important basis for more systematic analyses of cross-regulation of the DUX4 target gene network in the future.

Supplementary Material

Refer to Web version on PubMed Central for supplementary material.

Acknowledgement

The authors wish to acknowledge the support of the Chao Family Comprehensive Cancer Center Optical Biology Core (LAMMP/OBC) Shared Resource. We would also like to thank Dr. Naohiro Hashimoto (National Center for Geriatrics and Gerontology, Japan) for technical advice and Kevin Cabrera for helpful comments on the manuscript.

Funding information: This work was supported in part by National Institutes of Health (P01NS069539 to R.T., and R01AR071287 to K. Y. and A. M.).

Data availability statement:

All relevant data are within the paper and in supplemental figures.

References

Amini Chermahini G, Rashnonejad A, & Harper SQ (2019). RNAscope in situ hybridization-based method for detecting DUX4 RNA expression *in vitro*. RNA, 25, 1211–1217. [PubMed: 31209064]

Ansseau E, Laoudj-Chenivesse D, Marcowycz A, Tassin A, Vanderplanck C, Sauvage S, … Coppée F (2009). DUX4c is up-regulated in FSHD. It induces the MYF5 protein and human myoblast proliferation. PLoS One, 4(10), e7482. doi:10.1371/journal.pone.0007482 [PubMed: 19829708]

Bosnakovski D, Xu Z, Gang EJ, Galindo CL, Liu M, Simsek T, … Kyba M (2008). An isogenetic myoblast expression screen identifies DUX4-mediated FSHD-associated molecular pathologies. EMBO J., 27, 2766–2779. [PubMed: 18833193]

Broucqsault N, Morere J, Gaillard MC, Dumonceaux J, Torrents J, Salort-Campana E, … Roche S (2013). Dysregulation of 4q35- and muscle-specific genes in fetuses with a short D4Z4 array linked to facio-scapulo-humeral dystrophy. Hum. Mol. Genet, 22, 4206–4214. [PubMed: 23777630]

de Greef JC, Lemmers RJ, Camaño P, Day JW, Sacconi S, Dunand M, … Tawil R (2010). Clinical features of facioscapulohumeral muscular dystrophy 2. Neurol, 75, 1548–1554.

De Iaco A, Planet E, Coluccio A, Verp S, Duc J, & Trono D (2017). DUX-family transcription factors regulate zygotic genome activation in placental mammals. Nat. Genet, 49, 941–945. [PubMed: 28459456]

Deenen JC, Arnts H, van der Maarel SM, Padberg GW, Verschuuren JJ, Bakker E, … van Engelen BG (2014). Population-based incidence and prevalence of facioscapulohumeral dystrophy. Neurol., 83, 1056–1059.

Ferreboeuf M, Mariot V, Bessières B, Vasiljevic A, Attié-Bitach T, Collardeau S, … Dumonceaux J (2014). DUX4 and DUX4 downstream target genes are expressed in fetal FSHD muscles. Hum. Mol. Genet, 23, 171–181. [PubMed: 23966205]

Ferreboeuf M, Mariot V, Furling D, Butler-Browne G, Mouly V, & Dumonceaux J (2014). Nuclear protein spreading: implication for pathophysiology of neuromuscular diseases. Hum. Mol. Genet, 23, 4125–4133. [PubMed: 24659496]

Gabriëls J, Beckers MC, Ding H, De Vriese A, Plaisance S, van der Maarel SM, … Belayew A (1999). Nucleotide sequence of the partially deleted D4Z4 locus in a patient with FSHD identifies a putative gene within each 3.3 kb element. Gene, 236, 25–32. [PubMed: 10433963]

Geng LN, Yao Z, Snider L, Fong AP, Cech JN, Young JM, … Tapscott SJ (2012). DUX4 Activates Germline Genes, Retroelements, and Immune Mediators: Implications for Facioscapulohumeral Dystrophy. Dev. Cell, 22, 38–51. [PubMed: 22209328]

Hamanaka K, Šikrová D, Mitsuhashi S, Masuda H, Sekiguchi Y, Sugiyama A, … van der Maarel SM (2020). Homozygous nonsense variant in LRIF1 associated with facioscapulohumeral muscular dystrophy. Neurol., 94, e2441–e2447.

Hendrickson PG, Doráis JA, Grow EJ, Whiddon JL, Lim JW, Wike CL, … Cairns BR (2017). Conserved roles of mouse DUX and human DUX4 in activating cleavage-stage genes and MERVL/HERVL retrotransposons. Nat. Genet, 49, 925–934. [PubMed: 28459457]

Himeda CL, Jones TI, & Jones PL (2015). Facioscapulohumeral muscular dystrophy as a model for epigenetic regulation and disease. Antioxid. Redox. Signal, 22, 1463–1482. [PubMed: 25336259]

Homma S, Beermann ML, Boyce FM, & Miller JB (2015). Expression of FSHD-related DUX4-FL alters proteostasis and induces TDP-43 aggregation. Ann. Clin. Transl. Neurol, 2, 151–166. [PubMed: 25750920]

Jagannathan S, Shadle SC, Resnick R, Snider L, Tawil RN, van der Maarel SM, … Tapscott SJ (2016). Model systems of DUX4 expression recapitulate the transcriptional profile of FSHD cells. Hum. Mol. Genet, 25, 4419–4431. [PubMed: 28171552]

Jiang S, Williams K, Kong X, Zeng W, Ma X, Tawil R, … Mortazavi A (2020). Single-nucleus RNA-seq identifies divergent populations of FSHD2 myotube nuclei. PLoS Genet., 16, e1008754. doi:doi: 10.1371/journal.pgen.1008754. [PubMed: 32365093]

Jones TI, Chen JC, Rahimov F, Homma S, Arashiro P, Beermann ML, … Jones PL (2012). Facioscapulohumeral muscular dystrophy family studies of DUX4 expression: evidence for disease modifiers and a quantitative model of pathogenesis. Hum. Mol. Genet, 21, 4419–4430. [PubMed: 22798623]

Jouhilahti EM, Madissoon E, Vesterlund L, Töhönen V, Krjutškov K, Plaza Reyes A, … Kere J (2016). The human PRD-like homeobox gene LEUTX has a central role in embryo genome activation. Development, 143, 3459–3469. [PubMed: 27578796]

Katayama S, Ranga V, Jouhilahti EM, Airenne TT, Johnson MS, Mukherjee K, … Kere J (2018). Phylogenetic and mutational analyses of human LEUTX, a homeobox gene implicated in embryogenesis. Sci. Rep, 8, 17421. [PubMed: 30479355]

Larsen M, Rost S, El Hajj N, Ferbert A, Deschauer M, Walter MC, … Müller CR (2015). Diagnostic approach for FSHD revisited: SMCHD1 mutations cause FSHD2 and act as modifiers of disease severity in FSHD1. Eur. J. Hum. Genet, 23, 808–816. [PubMed: 25370034]

Lemmers RJLF, Tawil R, Petek LM, Balog J, Block GJ, Santen GWE, … van der Maarel SM (2012). Digenic inheritance of an SMCHD1 mutation and an FSHD-permissive D4Z4 allele causes facioscapulohumeral muscular dystrophy type 2. Nat. Genet, 44, 1370–1374. [PubMed: 23143600]

Lemmers RJLF, van der Vliet PJ, Klooster R, Sacconi S, Camaño P, Dauwerse JG, … van der Maarel SM (2010). A unifying genetic model for facioscapulohumeral muscular dystrophy. Science, 329, 1650–1653. [PubMed: 20724583]

Mainali KP, Bewick S, Thielen P, Mehoke T, Breitwieser FP, Paudel S, … Fagan WF (2017). Statistical analysis of co-occurrence patterns in microbial presence-absence datasets. PLoS One, 12, e0187132. [PubMed: 29145425]

Rahimov F, King OD, Leung DG, Bibat GM, Emerson CPJ, Kunkel LM, & Wagner KR (2012). Transcriptional profiling in facioscapulohumeral muscular dystrophy to identify candidate biomarkers. Proc. Natl. Acad. Sci, 109, 16234–16239. [PubMed: 22988124]

Rickard AM, Petek LM, & Miller DG (2015). Endogenous DUX4 expression in FSHD myotubes is sufficient to cause cell death and disrupts RNA splicing and cell migration pathways. Hum. Mol. Genet, 24, 5901–5914. [PubMed: 26246499]

Sacconi S, Lemmers RJ, Balog J, van der Vliet PJ, Lahaut P, van Nieuwenhuizen MP, … van der Maarel SM (2013). The FSHD2 Gene SMCHD1 Is a Modifier of Disease Severity in Families Affected by FSHD1. Am. J. Hum. Genet, 93, 744–751. [PubMed: 24075187]

Shadle SC, Zhong JW, Campbell AE, Conerly ML, Jagannathan S, Wong CJ, … Tapscott SJ (2017). DUX4-induced dsRNA and MYC mRNA stabilization activate apoptotic pathways in human cell models of facioscapulohumeral dystrophy. PLoS Genet., 13, e1006658. [PubMed: 28273136]

Shiomi K, Kiyono T, Okamura K, Uezumi M, Goto Y, Yasumoto S, … Hashimoto N (2011). CDK4 and cyclin D1 allow human myogenic cells to recapture growth property without compromising differentiation potential. Gene Ther., 18, 857–866. [PubMed: 21490680]

Sikandar SS, Pate KT, Anderson S, Dizon D, Edwards RA, Waterman ML, & Lipkin SM (2010). NOTCH signaling is required for formation and self-renewal of tumor-initiating cells and for repression of secretory cell differentiation in colon cancer. Cancer Res, 70, 1469–1478. [PubMed: 20145124]

Snider L, Asawachaicharn A, Tyler AE, Geng LN, Petek LM, Maves L, … Tapscott SJ (2009). RNA transcripts, miRNA-sized fragments and proteins produced from D4Z4 units: new candidates for the pathophysiology of facioscapulohumeral dystrophy. Hum. Mol. Genet, 18, 2414–2430. [PubMed: 19359275]

Snider L, Geng LN, Lemmers RJ, Kyba M, Ware CB, Nelson AM, … Miller DG (2010). Facioscapulohumeral dystrophy: incomplete suppression of a retrotransposed gene. PLoS Genet., 6, e1001181. [PubMed: 21060811]

Tassin A, Laoudj-Chenivesse D, Vanderplanck C, Barro M, Charron S, Ansseau E, … Belayew A (2013). DUX4 expression in FSHD muscle cells: how could such a rare protein cause a myopathy? J. Cell. Mol. Med, 17, 76–89. [PubMed: 23206257]

Tsumagari K, Chang SC, Lacey M, Baribault C, Chittur SV, Sowden J, … Ehrlich M (2011). Gene expression during normal and FSHD myogenesis. BMC Med. Genomics, 4, 67. [PubMed: 21951698]

van den Boogaard ML, Lemmers RJ, Balog J, Wohlgemuth M, Auranen M, Mitsuhashi S, … van der Maarel SM (2016). Mutations in DNMT3B Modify Epigenetic Repression of the D4Z4 Repeat and the Penetrance of Facioscapulohumeral Dystrophy. Am. J. Hum. Genet, 98, 1020–1029. [PubMed: 27153398]

van den Heuvel A, Mahfouz A, Kloet SL, Balog J, van Engelen BGM, Tawil R, … van der Maarel SM (2019). Single-cell RNA sequencing in facioscapulohumeral muscular dystrophy disease etiology and development. Hum. Mol. Genet, 28, 1064–1075. [PubMed: 30445587]

van der Maarel SM, & Frants RR (2005). The D4Z4 repeat-mediated pathogenesis of facioscapulohumeral muscular dystrophy. Am. J. Hum. Genet, 76, 375–386. [PubMed: 15674778]

van der Maarel SM, Tawil R, & Tapscott SJ (2011). Facioscapulohumeral muscular dystrophy and DUX4: breaking the silence. Trends Mol. Med, 17, 252–258. [PubMed: 21288772]

Vanderplanck C, Ansseau E, Charron S, Stricwant N, Tassin A, Laoudj-Chenivesse D, … Belayew A (2011). The FSHD atrophic myotube phenotype is caused by DUX4 expression. PLoS One, 6, e26820. [PubMed: 22053214]

Wang F, Flanagan J, Su N, Wang LC, Bui S, Nielson A, … Luo Y (2012). RNAscope: a novel *in situ* RNA analysis platform for formalin-fixed, paraffin-embedded tissues. J. Mol. Diagn, 14, 22–29. [PubMed: 22166544]

Whiddon JL, Langford AT, Wong CJ, Zhong JW, & Tapscott SJ (2017). Conservation and innovation in the DUX4-family gene network. Nat. Genet, 49, 935–940. [PubMed: 28459454]

Yao Z, Snider L, Balog J, Lemmers RJ, Van Der Maarel SM, Tawil R, & Tapscott SJ (2014). DUX4-induced gene expression is the major molecular signature in FSHD skeletal muscle. Hum. Mol. Genet, 23, 5342–5352. [PubMed: 24861551]

Zeng W, Jiang S, Kong X, El-Ali N, Ball J, A. R., Ma C, I.-H., … Mortazavi A (2016). Single-nucleus RNA-seq of differentiating human myoblasts reveals the extent of fate heterogeneity. Nuc. Acids Res, 44, e158.

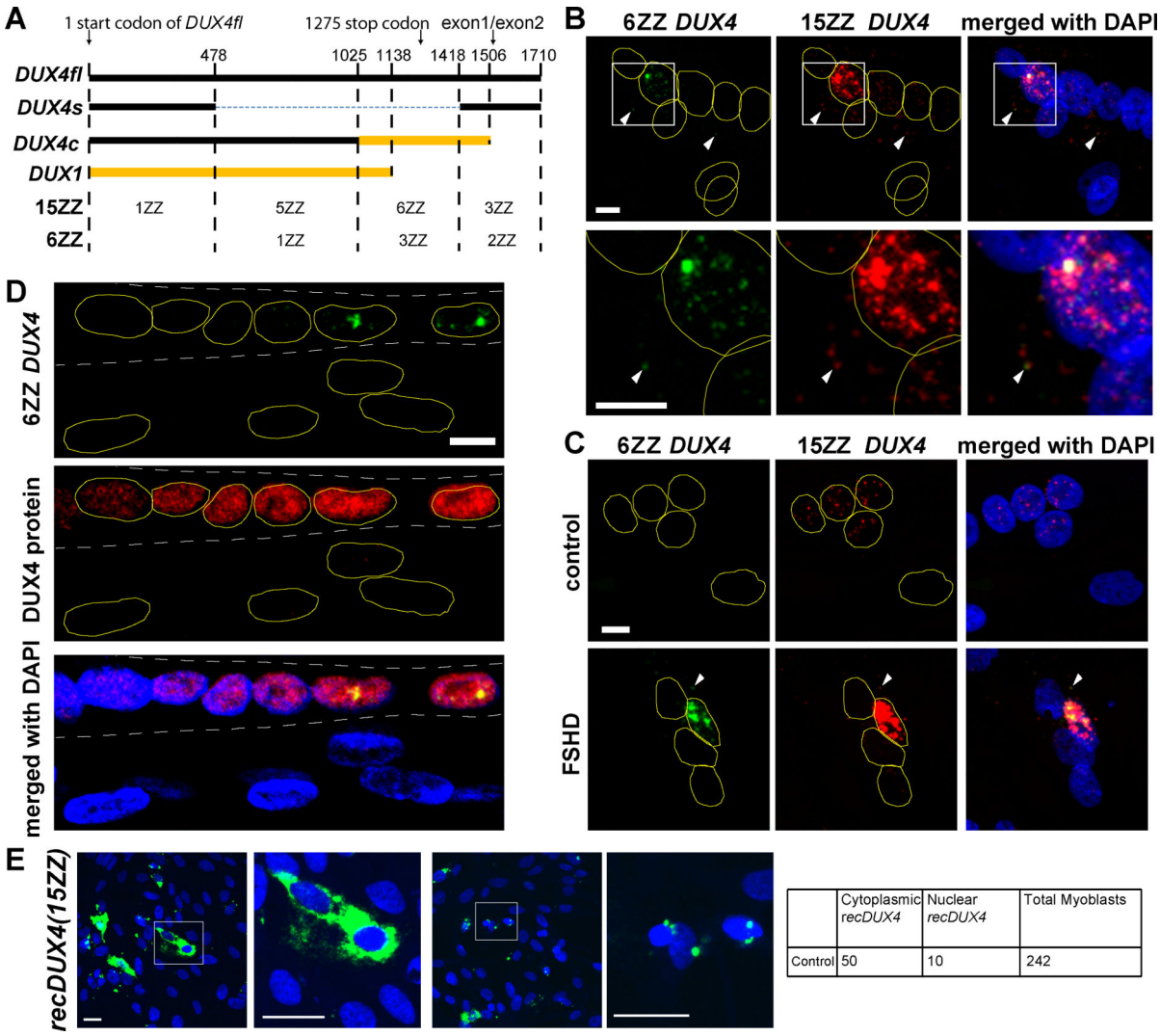

	Cytoplasmic *recDUX4*	Nuclear *recDUX4*	Total Myoblasts
Control	50	10	242

Figure 1. Specific detection of *DUX4* transcripts enriched in the FSHD myotube nucleus

A. Schematic diagram of mRNA transcripts for *DUX4fl,* the *DUX4s* isoform, *DUX4* homologs (*DUX4c* and *DUX1*), and the positions and numbers of individual ZZ pairs for the previously published RNAScope 15ZZ (Amini Chermahini et al., 2019) and our 6ZZ probe sets. The black regions of DUX4s and DUX4c represent >99% homology to *DUX4fl*, which can be cross-detected by corresponding ZZ pairs. The orange region in the 3' half of *DUX4c* and DUX1 were distinct and were confirmed not to crossreact with either 15ZZ or 6ZZ. As at least 3ZZ pairs are required for detectable signal, 15ZZ is capable of efficient detection of *DUX4s* (4ZZ total) and *DUX4c* (6ZZ total) (through the crosshybridization to the black regions). Our 6ZZ probe set was designed to preferentially detect *DUX4fl* and minimize the crossreactivity to *DUX4s* (2ZZ bind) and *DUX4c* (only 1ZZ binds). Numbers indicate nucleotide number from the 5' end of the transcripts. Nucleotide sequence comparison of four transcripts is shown in Supplemental Figure S1.

B. RNAScope costaining with 15ZZ and 6ZZ probe sets in FSHD myotubes at day 3 of differentiation. Colocalization of the nuclear foci detected by both 15ZZ and 6ZZ. The lower

panel is a magnification of the boxed region in the top panel. White arrowheads indicate the colocalization of both probe sets in the cytoplasm. Scale bar =10 μm.

C. Additional nuclear foci in control and FSHD myotubes.

Weak but distinct nuclear foci were observed in control cells with 15ZZ. No signal was observed with 6ZZ in control cells. Scale bar = 10 μm.

D. Immunofluorescent staining of DUX4 protein (red) and RNAScope detection of *DUX4* transcript using 6ZZ probes (green) in primary FSHD myotubes at day 7 of differentiation. DAPI is in blue. White dashed lines indicate the boundary of a myotube with positive DUX4 antibody staining signal. Scale bar = 10 μm.

E. RNAScope analysis of the transiently transfected recombinant *DUX4* (*recDUX4*) RNA expression in immortalized control myoblasts using 15ZZ. Example images and numbers of two different rec*DUX4* RNA localization patterns are shown. The boxes in the first column indicate where the image is zoomed in. Scale bar = 20 μm.

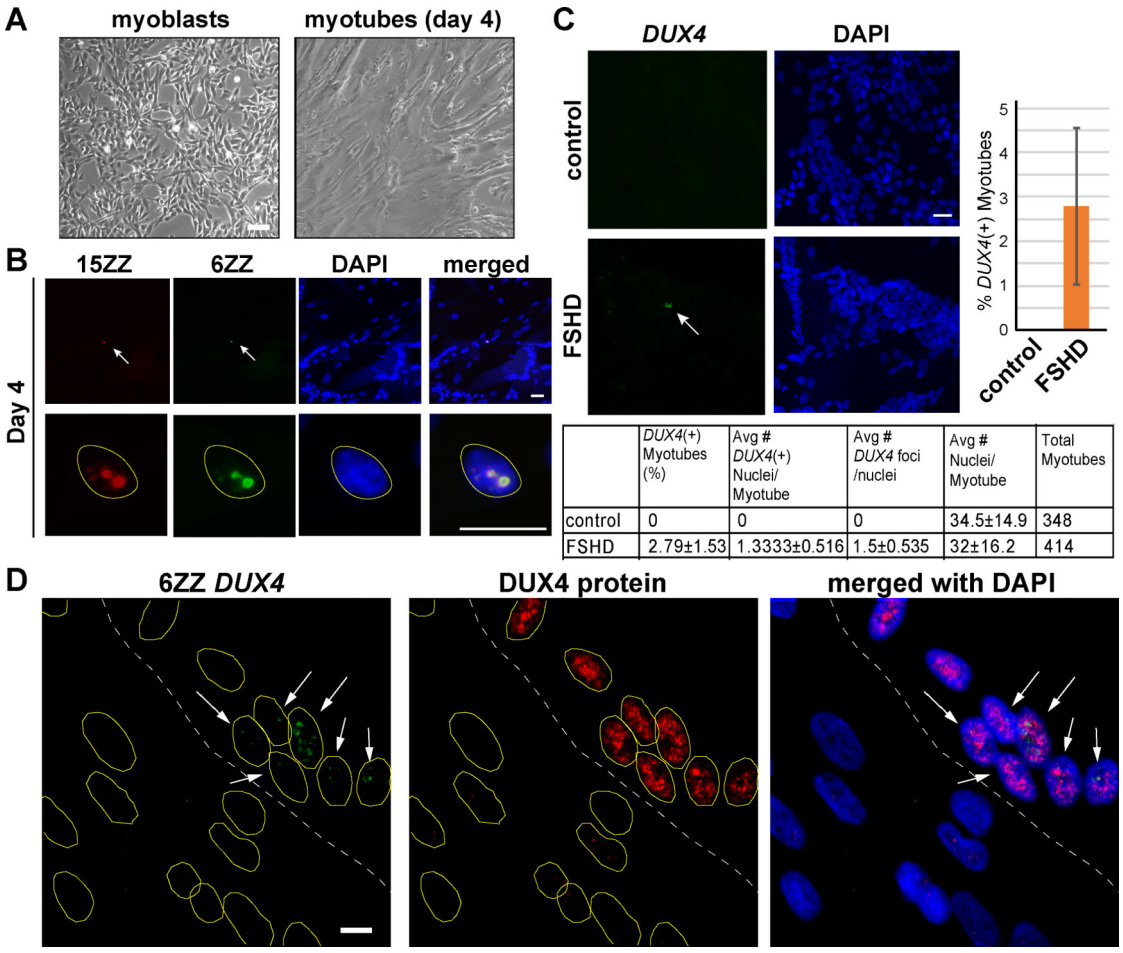

	DUX4(+) Myotubes (%)	Avg # DUX4(+) Nuclei/ Myotube	Avg # DUX4 foci /nuclei	Avg # Nuclei/ Myotube	Total Myotubes
control	0	0	0	34.5±14.9	348
FSHD	2.79±1.53	1.3333±0.516	1.5±0.535	32±16.2	414

Figure 2. *DUX4* transcripts upregulated in FSHD myotubes

A. Bright field images of immortalized clonal FSHD2 myoblast differentiation on day 0 and day 4. Scale bar=100 μm

B. RNAScope costaining of *DUX4* 15ZZ (red) and 6ZZ (green) probes in immortalized FSHD myotubes. White arrow indicates colocalization of probes. The lower panel is a magnification of the top panel. 15ZZ staining shows more foci and brighter signal similar to RNAScope staining in patient primary cells. Scale bar = 20 μm.

C. Characterization of *DUX4* 6ZZ RNAScope in day 3 immortalized control and FSHD myotubes. *DUX4* staining usually appears in the nucleus and has around 1–2 bright foci. Around 2.8% of 414 FSHD2 myotubes contained a positive *DUX4* RNAScope signal. Scale bar = 20 μm.

D. Detection of DUX4 protein by immunofluorescent staining and *DUX4* RNA by RNAScope. *DUX4* RNAScope (green) is combined with immunofluorescence using antibody against DUX4 (red) in immortalized FSHD myotubes at day 3 of differentiation. DAPI is in blue. White dashed line indicates the boundary of a myotube with positive DUX4 antibody staining signal. Arrow indicates nuclei with *DUX4* transcripts. Scale bar = 10 μm.

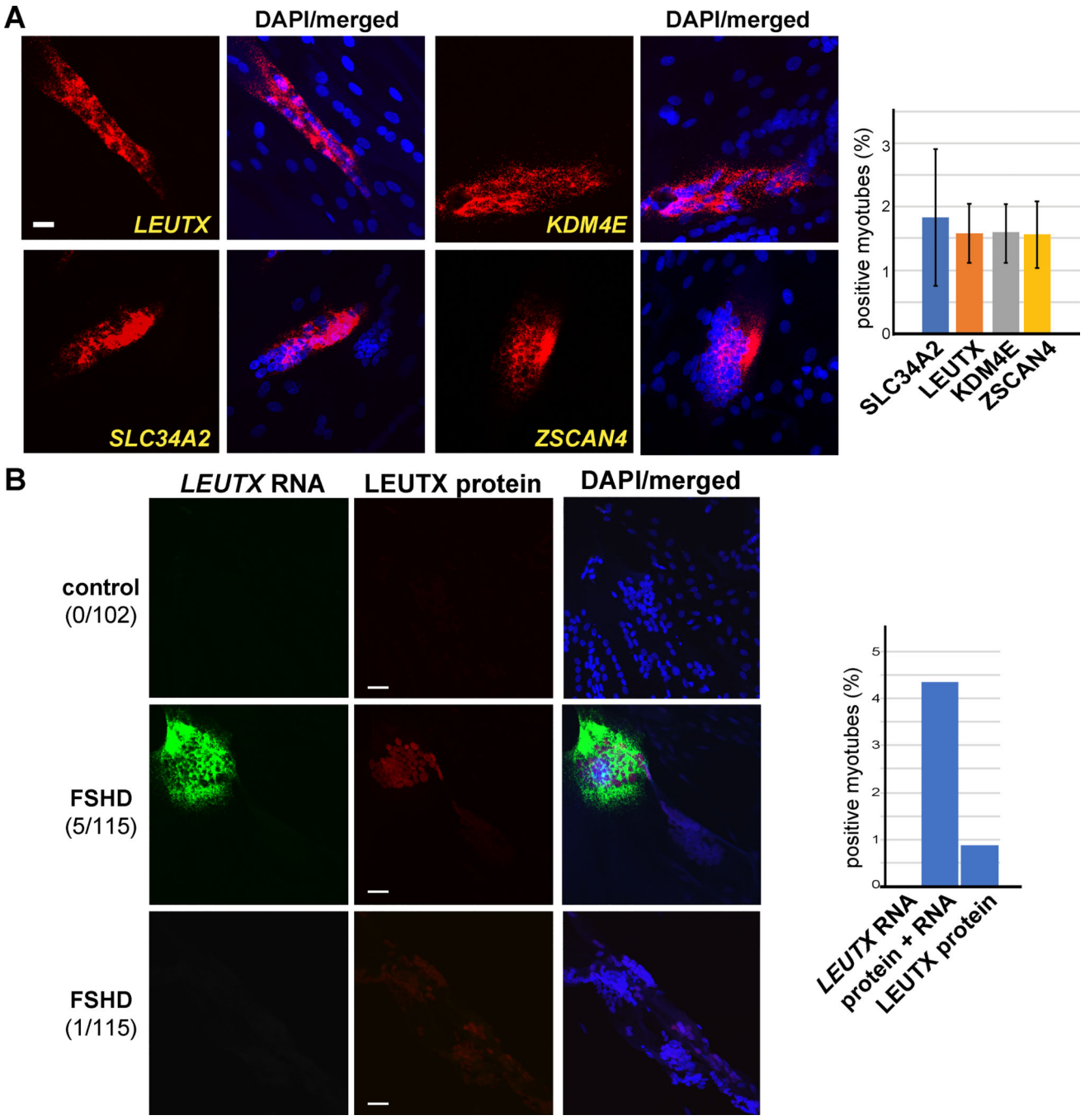

Figure 3. Comparison with DUX4 target gene expression

A. RNAScope staining of DUX4 target genes *LEUTX, KDM4E, SLC34A2*, and *ZSCAN4*. Merged images with DAPI (blue) staining are also shown as indicated at the top. Unlike *DUX4*, staining of target genes is spread along the myotube and in the cytoplasm. Approximately 2% of myotubes showed positive RNAScope target gene signal (right). Scale bar = 20 μm.

B. Costaining of *LEUTX* RNAScope (green) and LEUTX protein immunofluorescence staining (red) in control and FSHD myotubes on differentiation day 6. Merged images with

DAPI (blue) staining are also shown as indicated at the top. The middle panel shows a typical example of RNA and protein colocalization while the bottom panel shows an example of weak protein staining without RNA. Numbers of myotubes with corresponding patterns in the total myotubes counted are shown in parentheses. Percentages of myotubes with *LEUTX* RNA only, *LEUTX* RNA and protein, or LEUTX protein only are shown on the right. Scale bar = 20 μm.

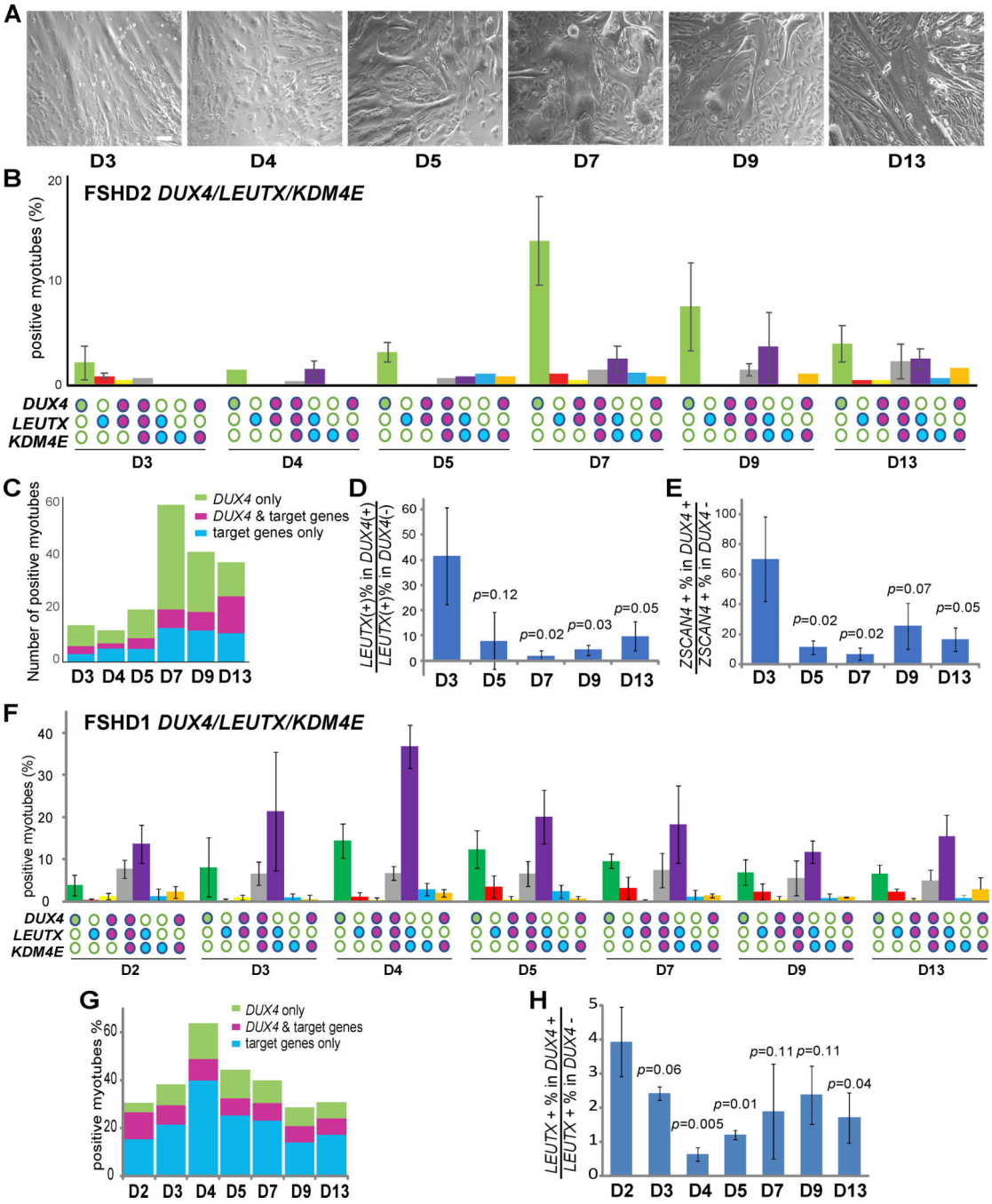

Figure 4.

Dynamic relationship between *DUX4* and target gene expression during myotube differentiation

A. Bright field images of immortalized FSHD myoblast differentiation into myotubes on days 3–13. Around day 5, we find greater myotube detachment. Scale bar =100 μm

B. Quantification of time course RNAScope triple staining of *DUX4*, *LEUTX*, and *KDM4E* transcripts. Error bars indicate the standard deviation from the mean of three independent experiments. The actual number counts are shown in Supplemental Figure S2.

C. Frequencies of myotubes expressing *DUX4 only*, *DUX4* and target genes, or target genes only change during differentiation. Replotting the data in (B) for the number of myotubes containing *DUX4* transcripts only, transcripts of DUX4 plus target gene(s), or transcripts of target gene(s) only as indicated. Y-axis is the total number of positive myotubes counted.
D. Frequency of *LEUTX* expression in *DUX4*-expressing myotubes decreases later in differentiation. The ratios between the percentage of *LEUTX*-expressing (LEUTX(+)) myotubes in the entire *DUX4*-expressing (DUX4(+)) myotubes and the percentage of LEUTX(+) myotubes in myotubes with no *DUX4* expression (*DUX4*(−)) at different days after differentiation were calculated based on the RNAScope data in (B). At day3, the frequency of DUX4(+) myotubes to co-express *LEUTX* is ~20–60 fold higher than the frequency of *DUX4*(−) myotubes to express LEUTX. Later in differentiation (days 7 and 9), the ratios drop significantly, indicating that the frequency of *LEUTX* expression without *DUX4* expression becomes more significant. The error bars represent the standard deviation of the mean of 3 independent experiments. The significance was evaluated by student t-test. The *p* values were calculated comparing to day 3. $p < 0.05$ was considered significant.
E. Frequency of *ZSCAN4* expression in *DUX4*-expressing myotubes decreases later in differentiation. The analysis was done as in (D) using the data in Supplemental Figure S3.
F. Quantification of time course RNAScope triple staining of *DUX4*, *LEUTX*, and *KDM4E* transcripts in immortalized FSHD1 myocytes. Error bars indicate the standard deviation from the mean of three independent experiments (see Supplemental Figure S4).
G. Replotting the data in (F) for frequencies of myotubes expressing *DUX4 only*, *DUX4* and target genes, or target genes only change during differentiation (similar to (C)). Y-axis is the percentage of positive myotubes as indicated relative to the total number of myotubes.
H. Frequency of *LEUTX* expression in *DUX4*-expressing myotubes changes during differentiation using the data in (F). The analysis was done as in (D).

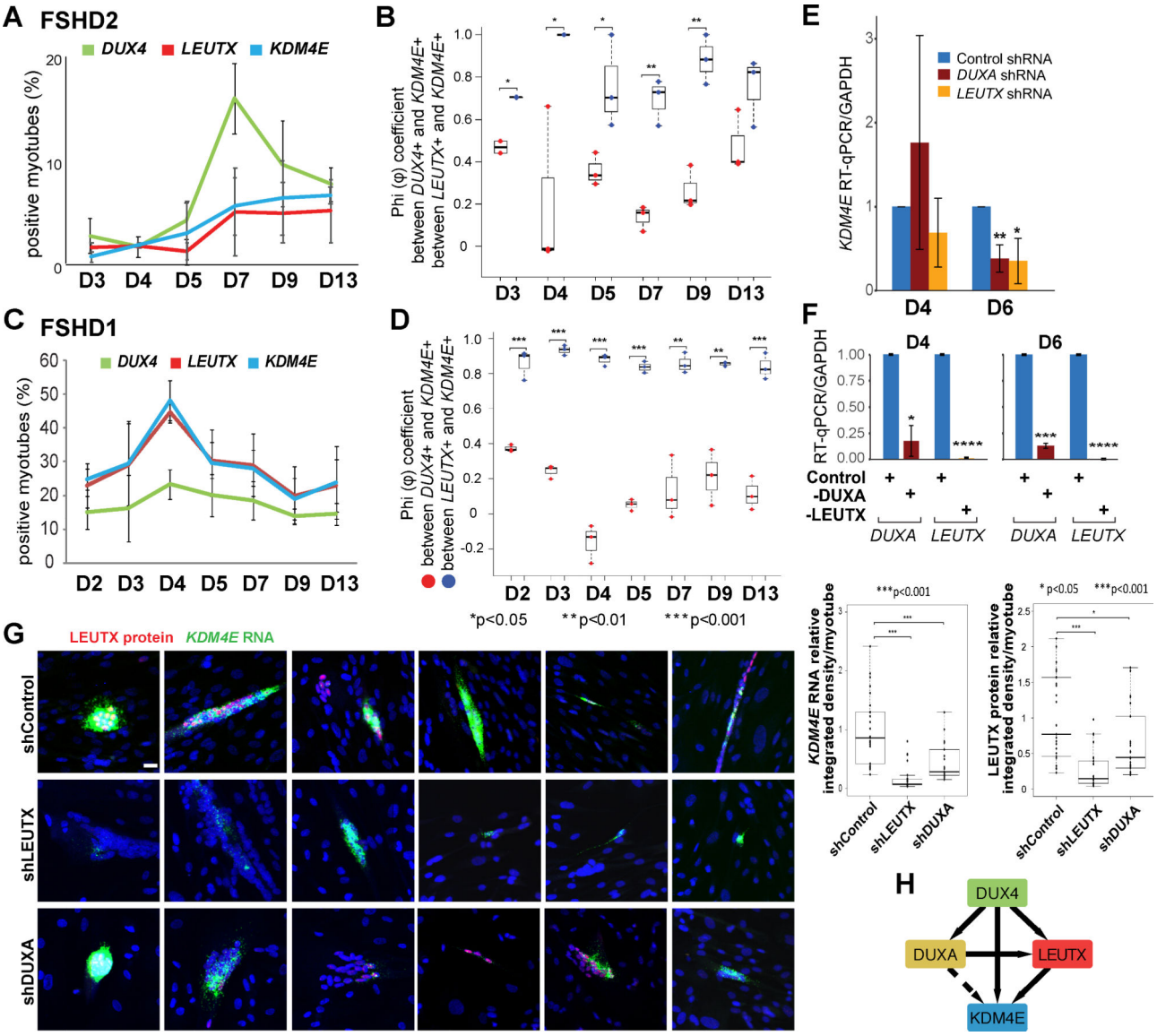

Fig. 5.

KDM4E expression is regulated by DUX4 target transcription factors

A. Individual time course RNAScope analysis of *DUX4, LEUTX*, and *KDM4E* in FSHD2 myotubes for the indicated days of differentiation from Figure 4B. These include all the positive myotubes for each transcript.

B. Comparison of correlation between *KDM4E* and *DUX4/LEUTX* expression based on the FSHD2 RNAScope data in Figure 4B. The high φ values indicate strong positive relationship between *KDM4E* and *LEUTX* RNA expression for the entire duration of the time course, with a perfect positive correlation (φ=1) on day 4. After that, the φ values decrease but are more significant than those between *KDM4E* and *DUX4* expression until day 13. P-values (unpaired, two-tailed t test) are for the correlation differences of indicated genes at the same day.

C. Individual time course RNAScope analysis of *DUX4, LEUTX*, and *KDM4E* in FSHD1 myotubes for the indicated days of differentiation from Figure 4F. These include all the positive myotubes for each transcript.

D. Comparison of correlation between *KDM4E* and *DUX4/ LEUTX* expression based on the FSHD1 RNAScope data in Figure 4F. The results indicate strong positive relationship between *KDM4E* and *LEUTX* RNA expression for the entire duration of the time course. The φ values between them are significantly higher than those between *KDM4E* and *DUX4* expression. P-values (unpaired, two-tailed t test) are for the correlation differences of indicated genes at the same day.

E. The effect of *DUXA* or *LEUTX* depletion on *KDM4E* expression in FSHD2 myotubes. *KDM4E* gene expression in control, *DUXA*, or *LEUTX* shRNA-treated myotubes on day 4 and day 6 was measured by RT-qPCR. The signal was normalized to *GAPDH*. The bar graph shows the average fold change of three independent experiments for each knockdown compared to the control shRNA-treated cells on day 4 or day 6 as indicated. Student t-test was used to calculate p-values. * p-value <0.05, ** p-value <0.01.

F. Analysis of depletion efficiency of *DUXA* and *LEUTX* shRNA by RT-qPCR for (E). Student t-test was used to calculate p-values for expression of *DUXA* or *LEUTX* in corresponding shRNA-treated myotubes compared to shRNA control on days 4 and 6 of differentiation. * p-value<0.05, *** p-value<0.001, **** p-value<0.0001.

G. Representative images of costaining of *KDM4E* RNAScope (green) and LEUTX antibody staining (red) in control, LEUTX, or DUXA shRNA-treated FSHD2 cells on differentiation day 6. Scale bar= 20 μm. Quantifications of *KDM4E* RNA and LEUTX protein are shown on the right (see methods for detail). * p-value <0.05, *** p-value <0.001.

H. A schematic diagram depicting the proposed relationship between DUX4 and the target genes. DUX4 expression is important for induction of *DUXA*, *LEUTX* and *KDM4E* during early FSHD myoblast differentiation. Once expressed, LEUTX contributes to *KDM4E* upregulation. DUXA activates *LEUTX* and *KDM4E* (directly and/or possibly through LEUTX).